*Journal of Naval Architecture and Marine Engineering*
*December, 2024*
http://dx.doi.org/10.3329/jname.v21i2.71364 *http://www.banglajol.info*

# MULTI-PHYSICAL ANALYSIS OF HEAT AND MASS TRANSFER IN VERTICAL CHANNEL WITH VARIABLE VISCOSITY, THERMAL CONDUCTIVITY AND THERMAL SLIP PHENOMENA

**Vanaja Gosty[1], G. Srinivas[2], B. Suresh Babu[1*]**
[1]Department of Mathematics, Sreyas Institute of Engineering and Technology, Hyderabad-500068, vanjag21@gmail.com
[2]Department of Mathematics, Geethanjali College of Engineering and Technology, Hyderabad-501301,gn.nivas@gmail.com
*Email: bsureshmaths@gmail.com

## Abstract:

*This research paper explores the intricacies of heat and mass transfer in a vertical channel with immiscible fluids, delving into the dynamics of two-fluid flows. The study investigates the impact of variable viscosity and thermal conductivity on the transfer processes within the channel. Additionally, the incorporation of thermal slip effects is considered, adding a layer of complexity to the analysis. The Runge-Kutta sixth-order method, implemented through Mathematica ND Solve technics, ensuring accurate numerical simulations. An extensive examination of dimensionless velocity, angular momentum, energy, and diffusion is performed across all pertinent parameters, and the results are graphically illustrated to draw meaningful conclusions. This visual representation simplifies the comparison of transfer rates along the channel wall. Bar charts visually represent key elements of heat and mass transfer, including shear stress, the Sherwood number, and the Nusselt number, to make it easier to compare transfer rates along the channel wall. The outcome has shown that there is a significant effect of pertinent parameters on both heat and mass transfer.*

***Keywords:*** Heat and mass transfer, vertical channel, immiscible fluids, variable viscosity, thermal slip, RK method.

**NOMENCLATURE**

| | |
|---|---|
| $U_1, U_2$ | Velocities in Region 1 and Region 2 |
| $U_0$ | Average Velocity |
| $T_1, T_2$ | Temperatures of the plate at $y = -h_1$ and $y = -h_2$ |
| $T_0$ | Average Temperature |
| $k_1, k_2$ | Thermal conductivity in Region 1 and Region 2 |
| $g$ | Acceleration due to gravity |
| $H_0$ | Magnetic Field Intensity |
| $st_1, st_2$ | Shear stress at $y = -h_1$ and $y = -h_2$ |
| $K$ | Vertex viscosity |

***Greek symbols***

| | |
|---|---|
| $\rho_1, \rho_2$ | Density of fluid in Region 1 and Region 2 |
| $\beta_1, \beta_2$ | Coefficient of Thermal expansion in Region 1 and Region 2 |
| $\mu_1, \mu_2$ | Viscosity of fluid in Region 1, Region 2 |
| $\sigma$ | Electrical conductivity |
| $\mu_e$ | Magnetic Field Permeability |

## 1. Introduction

Heat and mass transfer phenomena are integral to the functioning of numerous engineering applications, ranging from chemical processes to energy systems and environmental engineering. The continuous evolution of technology and the need for enhanced efficiency in these systems have sparked renewed interest in unraveling the intricacies of thermal and fluid dynamics in various configurations. Farooq et al . (2014) investigated the impact of physical parameters significantly influence mass and heat transport in vertical channels with two-layer flows of non-Newtonian fluid. Farooq et al. (2024) studied the flow of a fluid with varying viscosity and coupling tension between inclined plates, focusing on heat and mass transfer. Shah et al. (2024) analyze heat transfer in a magnetohydrodynamics-affected flow over a flexible Riga wall while considering the rate of entropy

1813-8535 (Print), 2070-8998 (Online)  Received on: January, 2024

development. Hwang et al. (2024) analyzed the process of heat transmission that occurs when condensation takes place on a vertical channel bundle with the inclusion of non-condensable gases. Jabeen et al. (2024) research takes bioconvection, activation energy, and viscous dissipation into account as it statistically examines the boundary layer flow of a Williamson nanofluid. Cheruku et al. (2023) explored Vertical channel flow of micropolar and viscous fluids, considering slip conditions for velocity, thermal, and diffusion are analyzed in the context of heat and mass transfer. Khan et al. (2023) examined the thermal and mass transfer in the movement of Williamson magnetohydrodynamic nanofluid over a large surface area.

Vertical channels are essential in engineering for heat and mass transfer, and they play a dynamic role in systems like heat exchangers. Their upright orientation is crucial in heat exchangers, condensers, and evaporators. An in-depth comprehension of fluid dynamics, thermal conduction, and mass diffusion in vertical channels is essential for achieving optimal system efficiency. These channels unique characteristics make them a focal point in designing and optimizing engineering systems requiring efficient heat and mass transfer. Khan et al. (2024) investigated the magnetohydrodynamic (MHD) behavior of a third-grade fluid as it flows through a vertical micro-channel containing with porous material. This study utilized the semi-implicit finite difference approach. Kalyan et al. (2023) examined the thermal and diffusion processes in two separate flows of Jeffrey fluid that do not mix, occurring within a vertical conduit. Babu et al. (2011) explored Thermal and mass transfer occur in the Vertical fluid flow within a channel through the utilization of the Finite Element Method (FEM).

Two-fluid flows introduce additional complexity, as interactions between different fluid phases significantly influence the overall transfer characteristics. This is particularly relevant in scenarios involving phase change, such as boiling or condensation, where the simultaneous presence of two fluid phases in a vertical channel poses intriguing challenges. Multiphase flow occurs many natural phenomena and it has many applications chemical industries and process industries. Leclaire et al. (2013) explores developments in lattice Boltzmann models, which are used to simulate the behavior of immiscible fluid mixtures, or components with different viscosities and densities. Xu, h et al. (2024) examines and contrasts the merging of droplets that do not mix together in liquids with different levels of thickness with their miscible counterparts using experimental research. Bashir et al. (2023) investigated the dynamics of two immiscible layers of micropolar and viscous fluids that rotate evenly. Suresh Babu et al. (2019) examined the thermodynamic and fluid dynamic Fluid dynamics in a channel with varying width in a vertical orientation, taking into account the influence of the Soret and Dufour effects. Huang, Hulin, et al. (2024) Researchers in the field of bioengineering study how mass and heat move through multilayered flows that have two fluids that don't mix and are moved by beating cilia. Potyka, et al. (2024) investigated a three-dimensional direct numerical simulation using the volume of fluid method to study collisions between immiscible droplets. Bandari et al. (2023) Investigate radial vibrations in a cylindrical bore that is poroelastic and filled with two immiscible fluids. Alyousef et al. (2023) explored the mathematical modeling and analysis of continual electro-osmotic flow between two immiscible fluids.

Fluids with varying viscosity and thermal conductivity find extensive applications in numerous engineering projects. Such fluids, for example, can undergo analysis in operational scenarios involving high temperatures, pressure, shear rate, etc., especially in examining lubricants. Makinde (2012) the impact of radiation, variable viscosity, and suction and insertion are factors that could significantly influence heat transfer analyses in various scenarios. Baitharu et al. (2021) examining convective heat transmission in stretching/shrinking within the framework of magneto-fluid dynamics while considering the impacts of changing viscosity, thermal conductivity, and heat source. Ullah et al. (2023) investigated how viscosity variations affect oscillatory mass and heat transfer in mixed convective flow with chemical processes across an inclined hot plate in a low-gravity environment. Pal, D et al. (2014) consider the effects of varying heat conductivity and viscosity on the non-free convective flow across a stretched sheet in a confined scenario. Hazarika et al. (216) over a stretched surface with heat radiation, considering injection. Hazarika et al. (2016) study examined how temperature-dependent magnetohydrodynamic flow and heat transfer over a stretching plate in a porous material are influenced by its viscosity and thermal conductivity. The study took into account factors such as radiation, thermal production, and dissipation of Joules. The analysis of thermal slip is essential for understanding two-fluid flows, indicating relative motion between fluid phases caused by temperature disparities. This phenomenon significantly impacts heat transfer rates between phases, emphasizing the importance of measuring thermal slip to optimize the performance of systems involving multiple fluid phases. Cheruku et al. (2023) explores thermal slip in vertical channel immiscible micropolar and viscous fluid flow. Increased thermal slip is observed to lead to a reduction in both velocity profile and temperature. Mahmood, Zafar, et al . (2024) studied the effects of changes in the slip velocity, mixed convection of nanofluids on the behavior of a stretching surface are demonstrated in this experiment. Kho, Yap Bing, et al.

(2019) variables, including the velocity, thermal slip, and non-Newtonian Williamson component are looked at, the Nusselt number goes down as the Lewis and Prandtl numbers go up. Malapati et al. (2021) performed on the thermal slips in the Williamson nanofluid boundary layer across a stretching sheet. Abbas et al. (2023) investigate the flow of micropolar nanofluid across a vertically stretched nonlinear Riga sheet and find that higher thermal slip values cause a drop in the Nusselt and Sherwood numbers. Reddy et al. (2023) at the stagnation point, investigate the influence of porosity, radiation, and viscous dissipation on two-dimensional unsteady magnetohydrodynamic mixed convection heat and mass transfer flow. Kiran Kumar et al. (2019) investigates the influence of different fluid viscosities and thermal conductivities on magnetohydrodynamic (MHD) flow and heat transfer in a vertical channel containing a heat source, while considering the presence of thermal slip. Ganesh et al. (2019) numerical simulation of Newtonian fluid flow including buoyancy effects, second-order thermal slip, and entropy generation demonstrates that increasing the Soret number reduces temperature via boosting fluid-particle diffusion. Goud et al. (2022) investigated the magnetohydrodynamic flow of a micropolar fluid over a vertical porous plate that is in motion, taking into account thermal radiation.

In this study, heat and mass transfer occur in a vertical channel that contains immiscible micropolar and viscous fluids. Factoring in boundary slip conditions. Our focus is specifically on exploring the influence of slip effect on temperature, as well as the variations in thermal conductivity and viscosity, on the relevant parameter. The RK 6$^{th}$ order approach, executed with ND Solve technique in Mathematica, guarantees precise numerical simulations. This research endeavors can offer crucial information for maximizing heat and mass transfer processes in various engineering applications. The validation of the problem is ensured by comparing the present work with earlier studies ignoring the crux parameters.

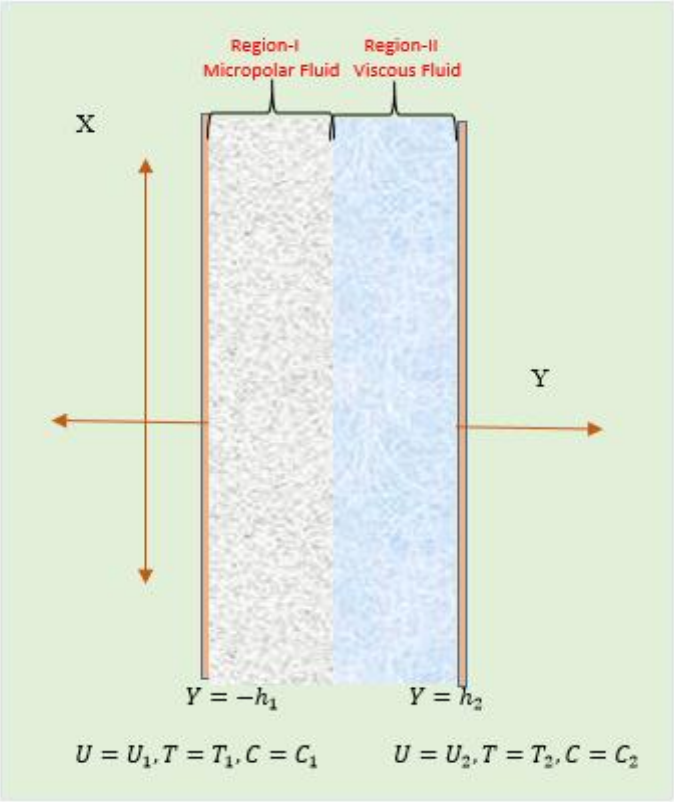


Fig. 1: Geometry of the Problem

## 2. Mathematical Formulation

To derive the governing equations, the vertical channel considered as bounded by walls kept at $Y=-h_1$ and $Y=h_2$ along the Y-axis, as illustrated in Figure 1. The channel contains two non-uniform-temperature plates denoted as $T_1$ and $T_2$, where $T_1 > T_2$. The Region-1 spans from $Y=-h_1$ to $Y=0$ and is filled with a micropolar fluid and the Region-2 spans from $Y=0$ to $Y=h_2$ and filled with viscous fluid. The flow is assumed to be one-dimensional, steady, laminar, incompressible, and immiscible. The Fluid motion by buoyancy forces. Also the transport

properties are fixed and flow model is fully developed. The continuity conditions hold at the interface for the governing parameters. The Boussinesq approximation is employed to model the flow.

The equations governed by the flow, heat and mass transfer with the above assumptions are:

**Region-1**

$$\frac{\partial U_1}{\partial Y} = 0 \tag{1}$$

$$\rho_1 = \rho_0[1 - \beta_{1T}(T_1 - T_*) - \beta_{1C}(C_1 - C_*)] \tag{2}$$

$$\frac{1}{\rho_1}\frac{\partial}{\partial Y}\left((\mu_1 + K)\frac{\partial U_1}{\partial Y}\right) + \frac{K}{\rho_1}\frac{\partial N}{\partial Y} + g\beta_{1T}(T_1 - T_*) + g\beta_{1C}(C_1 - C_*) - \sigma\frac{A_0^2 U_1}{\rho_1} = 0 \tag{3}$$

$$\gamma\frac{\partial^2 N}{\partial Y^2} - K\left(2N + \frac{\partial U_1}{\partial Y}\right) = 0 \tag{4}$$

$$\frac{1}{\rho C_P}\left[\frac{\partial}{\partial Y}k_1\frac{\partial T_1}{\partial Y} + \mu_1\left(\frac{\partial U_1}{\partial Y}\right)^2 + \frac{\rho_1 D_1 K_{T1}}{C_{s1}}\frac{\partial^2 C_1}{\partial Y^2}\right] = 0 \tag{5}$$

$$D_1\frac{\partial^2 C_1}{\partial Y^2} + \frac{D_1 K T_1}{T_m}\frac{\partial^2 T_1}{\partial Y^2} = 0 \tag{6}$$

**Region-2**

$$\frac{\partial U_2}{\partial Y} = 0 \tag{7}$$

$$\frac{1}{\rho_2}\frac{\partial}{\partial Y}(\mu_2)\frac{\partial U_2}{\partial Y} + g\beta_{2T}(T_2 - T_*) + g\beta_{2c}(C_2 - C_*) - \sigma\frac{B_0^2 U_2}{\rho_2} = 0 \tag{8}$$

$$\frac{1}{\rho_2 C_P}\left[\frac{\partial}{\partial Y}k_2\frac{\partial T_2}{\partial Y} + \mu_2\left(\frac{\partial U_2}{\partial Y}\right)^2 + \frac{\rho_2 D_2 K_{T2}}{C_{s2}}\frac{\partial^2 C_2}{\partial Y^2}\right] = 0 \tag{9}$$

$$D_2\frac{\partial^2 C_2}{\partial Y^2} + \frac{D_2 K T_2}{T_m}\frac{\partial^2 T_2}{\partial Y^2} = 0 \tag{10}$$

Boundary and interface conditions

$U = 0\ at\ Y = -h_1,\ U = 0\ at\ Y = h_2,$

$T = T_* + A\frac{\partial T_1}{\partial y}\ atY = -h_1,$

$T = T_2\ at\ Y = h_2,\ \frac{dN}{dY} = 0\ at\ Y = 0$

$C = 1$ at $Y = -h_1, C = C_2$ at $Y = h_2$

$U_1 = U_2\ at\ Y = 0,$

$T_1 = T_2\ at\ Y = 0,$

$C_1 = C_2\ at\ Y = 0,$

$\frac{dU_1}{dY} = 0\ at\ Y = 0, \frac{dU_2}{dY} = 0\ at\ Y = 0,$

$\frac{dT_1}{dY} = 0\ at\ Y = 0, \frac{dT_2}{dY} = 0 at\ Y = 0,$

$\frac{dC_1}{dY} = 0\ at\ Y = 0,$

$\frac{dC_2}{dY} = 0\ at\ Y = 0$ (11)

## Non-dimensional Variables

$y = \frac{Y}{h_1}$ (Region 1), $u_1 = \frac{U_1}{U_0}$ , $\theta_1 = \frac{T_1 - T_*}{\Delta T}$, $\phi_1 = \frac{C_1 - C_*}{\Delta C}$, $y = \frac{Y}{h_2}$ (Region 2),

$u_2 = \frac{U_2}{U_0}$, $\theta_2 = \frac{T_2 - T_*}{\Delta T}$, $\phi_2 = \frac{C_2 - C_*}{\Delta C}$, $a = \frac{A}{h_1}$

The PDE system is converted to a form that has no dimensions by utilizing the variables listed below:

$M = \frac{\sigma {A_0}^2 {h_1}^2}{\mu_\infty}$ (Magnetic field parameter), $Gr = \frac{g\beta_{1T}\Delta T {h_1}^3}{{\nu_1}^2}$ (Grashof number),

$\nu_1 = \frac{\mu_\infty}{\rho_1}$, $R = \frac{U_0 h_1}{\nu_1}$ (Reynolds number), $Pr = \frac{\nu_1}{\alpha_0}$, $Ec = \frac{{U_0}^2}{Cp_1 \Delta T}$ (Eckert number),

$h = \frac{h_1}{h_2}$, $Cp = \frac{Cp_1}{Cp_2}$, $\nu_2 = \frac{\mu_\infty}{\rho_2}$, $\alpha_2 = \frac{k_2}{\rho_2 Cp_2}$, $U_0$ is characteristic velocity of fluid.

$\mu_1 = -\frac{\mu_\infty \theta_r}{\theta_1 - \theta_r}$ and $\mu_2 = -\frac{\mu_\infty \theta_r}{\theta_2 - \theta_r}$ for regions 1 and 2 respectively,

Therefore the governing equations can be transformed into a non-dimensional form in the following manner:

**Region-1:**

$$\frac{\partial^2 u_1}{\partial y^2} - \frac{2k}{2+k}\left(2n + \frac{\partial u_1}{\partial y}\right) = 0 \tag{12}$$

$$\mathrm{K}\frac{\partial n}{\partial y} + \frac{\theta_r}{(\theta_1 - \theta_r)^2}\frac{\partial \theta_1}{\partial y}\frac{\partial u_1}{\partial y} - \frac{\theta_r}{(\theta_1 - \theta_r)}\frac{\partial^2 u_1}{\partial y^2} + \frac{G_r}{R}\theta_1 + \frac{Gc}{R}\phi_1 - Mu_1 = 0 \tag{13}$$

$$\beta_1 \left(\frac{\partial \theta_1}{\partial y}\right)^2 + (1 + \beta_1 \theta_1)\frac{\partial^2 \theta_1}{\partial y^2} - Pr\, E_c \left(\frac{\theta_r}{\theta_1 - \theta_r}\right)\left(\frac{\partial u_1}{\partial y}\right)^2 = 0 \tag{14}$$

$$\frac{1}{S_c R}\frac{\partial^2 \phi_1}{\partial y^2} + S_r \frac{\partial^2 \theta_1}{\partial y^2} = 0 \tag{15}$$

**Region -2**

$$\frac{\theta_r}{(\theta_2 - \theta_r)^2}\frac{\partial \theta_2}{\partial y}\frac{\partial u_2}{\partial y} - \frac{\theta_r}{(\theta_2 - \theta_r)}\frac{\partial^2 u_2}{\partial y^2} + \frac{1}{a_1 b_1 f^2}\frac{G_r}{R}\theta_2 + \frac{1}{a_1 b_1 f^2}\frac{G_c}{R}\phi_2 - Mu_2 = 0 \tag{16}$$

$$\beta_2 \left(\frac{\partial \theta_2}{\partial y}\right)^2 + (1 + \beta_2 \theta_2)\frac{\partial^2 \theta_2}{\partial y^2} - a\, Pr\, E\, c \left(\frac{\theta_r}{\theta_2 - \theta_r}\right)\left(\frac{\partial u_2}{\partial y}\right)^2 = 0 \tag{17}$$

$$\frac{f}{dS_c R}\frac{\partial^2 \phi_2}{\partial y^2} + \frac{fS_r}{KTd}\frac{\partial^2 \theta_2}{\partial y^2} = 0 \tag{18}$$

Similarly (11) will be converted to the following dimensionless form:

$u_1 = 0$ at $y = -1$

$\theta_1 = 1 + a\left(\frac{\partial \theta_1}{\partial y}\right)\ at\ y = -1$

$\phi_1 = 1$ at $y = 1, n = 0$ at $y = -1$

$\frac{\partial n}{\partial y} = 0\ at\ y = 0,$

$u_1 = u_2\ at\ y = 0,$

$\theta_1 = \theta_2\ at\ y = 0$

$\phi_1 = \phi_2 at\ y = 0\ ,\ \frac{\partial u_2}{\partial y} = mh\frac{\partial u_1}{\partial y}\ at\ y = 0$

$\frac{\partial \theta_2}{\partial y} = h\alpha\frac{\partial \theta_1}{\partial y}\ at\ y = 0,$

$\frac{\partial \phi_2}{\partial y} = df\frac{\partial \phi_1}{\partial y}\ at\ y = 0$

$u_2 = 0\ at\ y = 1$

$\theta_2 = 0\ at\ y = 1,\ \ \phi_2 = 0\ at\ y = 1$

## 3. Solution of the Problem

The numerical solutions to the nonlinear equations are obtained using the sixth-order Runge-Kutta method and Mathematica ND Solve techniques. Various important parameters are determined through these numerical methods, including the thermal Grashof number (Gr), the molecular Grashof number (Gc), the Reynolds number (R), the magnetic field parameter (M), the material parameter (K), the Schmidt number (Sc), the Soret number (Sr), variable viscosity ($\theta_r$), thermal slip (a).The impact of these dimensionless parameters on velocity, angular velocity, temperature, and diffusion is analyzed and illustrated with graphical representations.

Also the rate of velocity, heat and mass transfer are calculated using the following formulae:

$Nu_1 = \left[\frac{\partial \theta_1}{\partial y}\right]_{y=-1}, Nu_2 = \left[\frac{\partial \theta_2}{\partial y}\right]_{y=1},\ St_1 = \left[\frac{\partial u_1}{\partial y}\right]_{y=-1}, St_2 = \left[\frac{\partial u_2}{\partial y}\right]_{y=1},$

$Sh_1 = \left[\frac{\partial \phi_1}{\partial y}\right]_{y=-1},\ Sh_2 = \left[\frac{\partial \phi_2}{\partial y}\right]_{y=1}$

## 4. Results and Discussion

The solution to nonlinear partial differential equations, coupled with their associated boundary conditions, was achieved through the application of the Runge-Kutta sixth-order method and Mathematica ND Solve software. A

comprehensive computational analysis was undertaken to elucidate the influence of critical physical parameters—including Grashof number (Gr), molecular Grashof number (Gc), material parameter (k), Reynolds number (R), magnetic field parameter (M), Sorret number (Sr), Smidth number (Sc), Variable viscosity ($\theta$r), and the thermal slip parameter (a)—on key physical variables such as velocity, angular velocity, temperature, and diffusion.

Figures 2-9 demonstrate the changes on velocity of various parameters, Figures 2, 3 and 8 illustrate a Grashof number (Gr), molecular Grashof number (Gc), and variable viscosity ($\theta$r) result in an increase in fluid velocity. This phenomenon emerges from the intricate interaction among various components in the field of fluid dynamics. The Grashof number quantifies the relative influence of buoyant and viscous forces in fluid flow, where higher values of Gr indicate a greater dominance of buoyancy. The molecular Grashof number (Gc) takes into account the molecular conductivity, improving our comprehension of heat transport. The increase of Gc lead to reversal flow in the second region due to effect of thermal slip on viscous fluid. Enhanced thermal conductivity enhances the efficiency of heat transport in the fluid. The combined effects significantly increase the velocity of the fluid, illustrating the intricate interplay between various thermal properties, buoyancy forces, and the principles of fluid dynamics. This enhanced speed showcases how changes in temperature can influence buoyancy, which in turn affects the movement and behavior of the fluid within the system. The relationship between these factors is complex, as they each contribute to the overall dynamics in a way that highlights the sophisticated nature of thermal-fluid interactions.

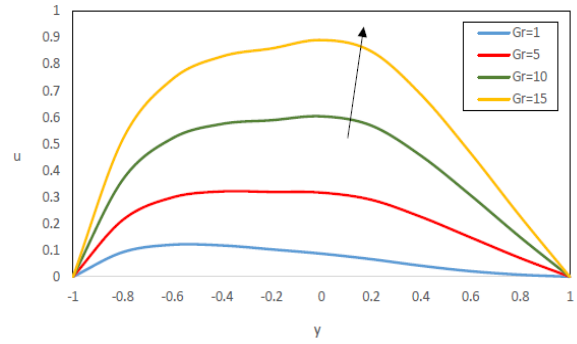


Fig. 2: Variation of velocity with Gr

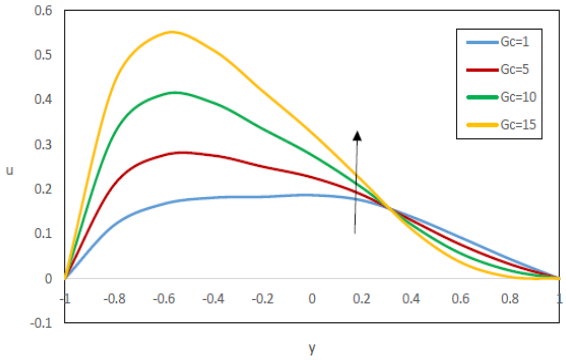


Fig. 3: Variation of velocity with Gc

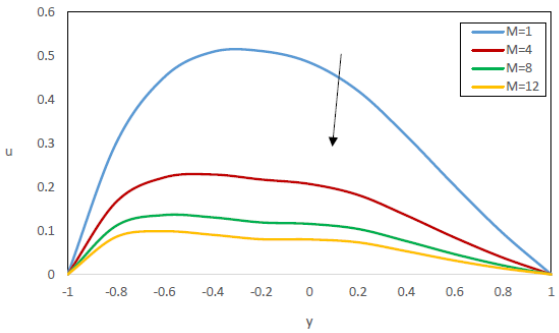


Fig. 4: Variation of velocity with M.

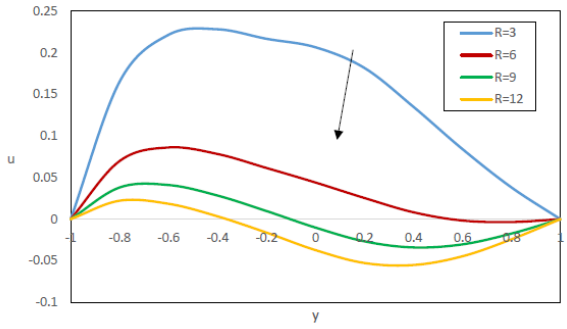


Fig. 5: Variation of velocity with R

Figures 4-7 and 9 illustrate the magnetic field parameter (M), Reynolds number (R), Sorret number (Sr), Smidth number (Sc), and thermal slip (a) corresponds to a reduction in the velocity of a fluid. This phenomenon arises due to the intricate relationships among these parameters in the context of magnetohydrodynamics and thermal slip effects. The increase in magnetic field parameter M intensifies magnetic forces, suppressing fluid motion. Concurrently, a higher Reynolds number implies increased inertia, posing a challenge for magnetic forces to overcome the fluid's momentum. Elevated Sorret number (Sr), Smidth number (Sc), and thermal slip (a) contribute to heightened thermal effects and diminished momentum transfer, collectively resulting in a decline in fluid velocity. This intricate interplay underscores how alterations in magnetic, thermal, and flow parameters collectively shape the dynamic behavior of the fluid, resulting in a reduction in velocity.

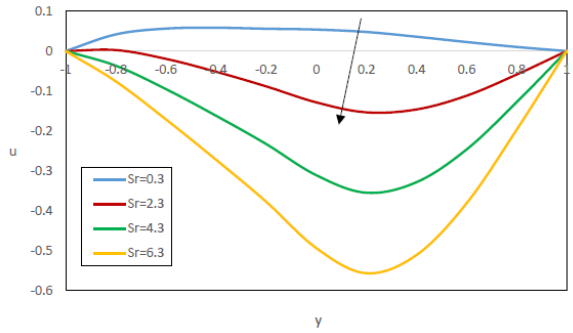


Fig. 6: Variation of velocity with Sr

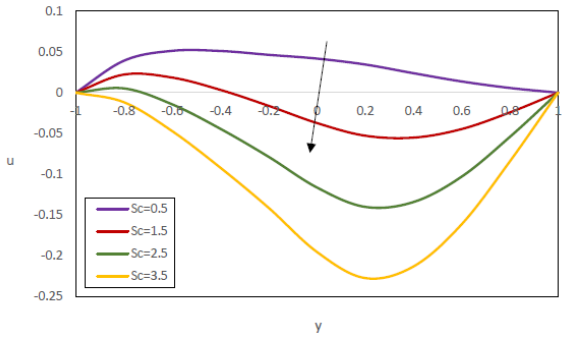


Fig. 7: Variation of velocity with Sc

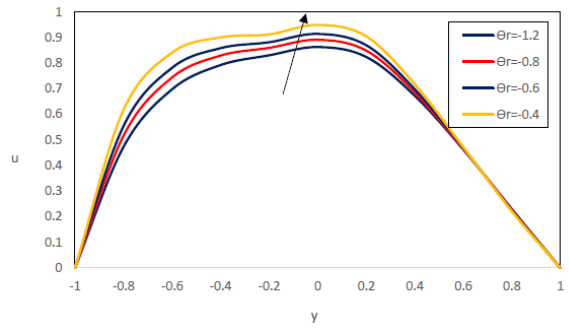


Fig. 8: Variation of velocity with $\Theta$r

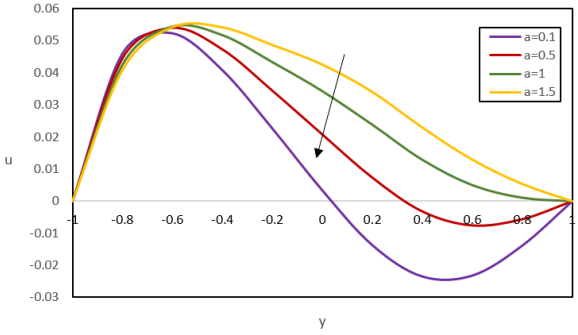


Fig. 9: Variation of velocity with Thermal slip (a)

The angular velocity is shown in figures 10–17. The molecular Grashof number, magnetic field parameter, Reynolds number, Sorret number, Smidth number, and Variable viscosity are shown in Figures 11–16. As these parameters grow, the angular velocity tends to increase, indicating an intricate interaction between fluid dynamics and magnetohydrodynamics. The higher molecule Grashof number intensifies the buoyancy effect, leading to an increase in fluid velocity. Simultaneously, a rise in magnetic field strength (M) amplifies magnetic forces, leading to greater angular momentum. A higher Reynolds number (R) indicates a transition to a more turbulent flow, leading to an increase in angular velocity. Higher Sorret number (Sr), Smidth number (Sc), and thermal conductivity all work together to improve thermal effects and momentum transfer, which leads to an overall increase in angular velocity. The complex interplay of chemical, magnetic, and flow factors has a collective impact on the system's angular dynamics. Figures 10 and 17 demonstrate a negative correlation between the Grashof number, thermal slip, and the angular velocity of the system. The Grashof number, which represents the balance between viscous and buoyant forces, promotes fluid motion as it increases. On the other hand, when there is increased thermal slip, it means that there is less thermal interaction with the boundary. This hampers the effective transmission of heat and reduces the forces caused by buoyancy. Therefore, when the Grashof number is high and there is thermal slip, the fluid's ability to maintain rotational motion is limited, leading to a decrease in angular velocity.

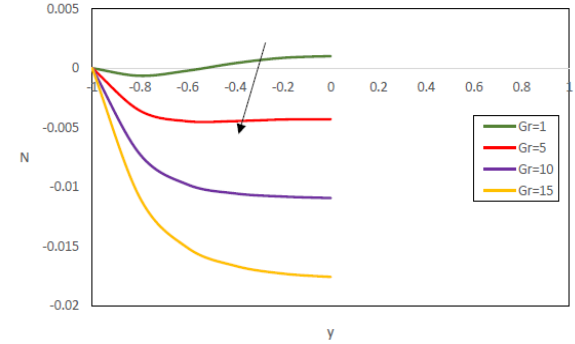


Fig. 10: Variation of angular velocity with Gr

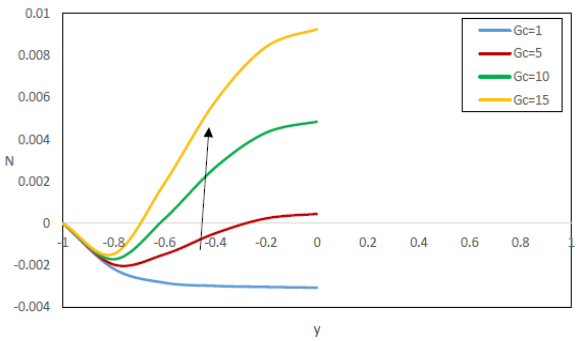


Fig. 11: Variation of angular velocity with Gc

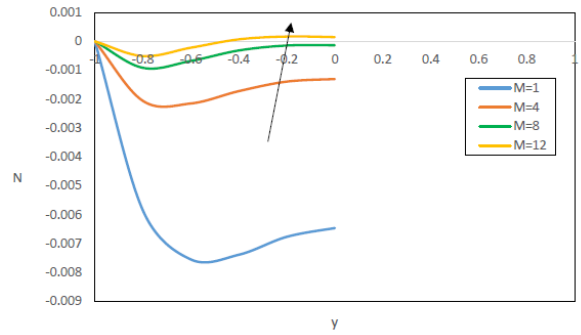


Fig. 12: Variation of angular velocity with M

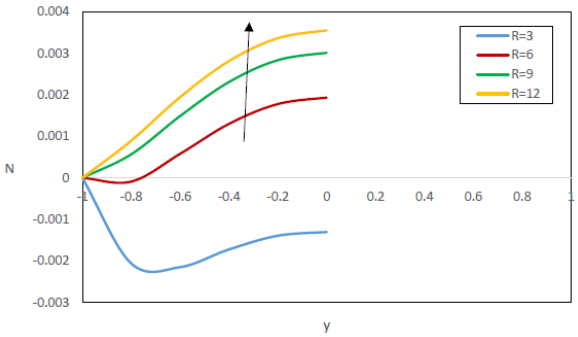


Fig. 13: Variation of angular velocity with R

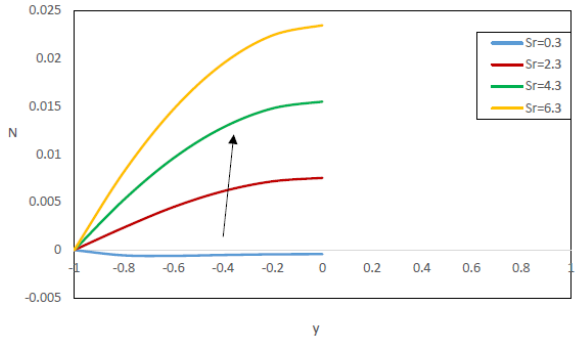


Fig. 14: Variation of angular velocity with Sr

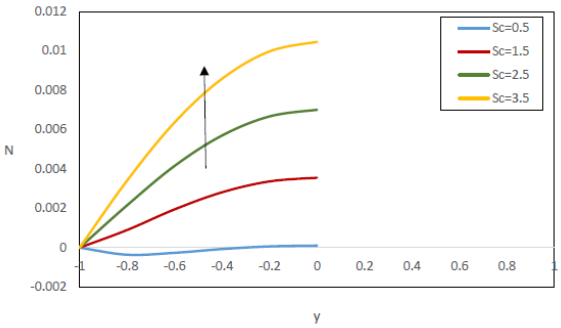


Fig. 15: Variation of angular velocity with Sc

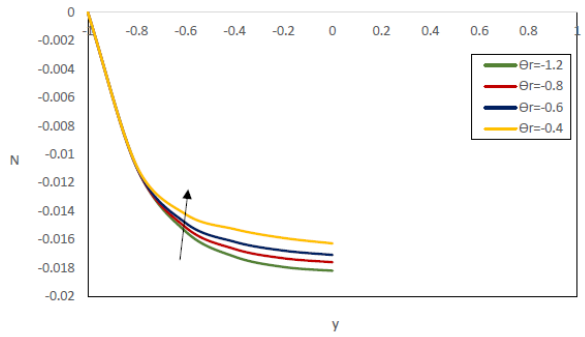


Fig. 16: Variation of angular velocity with $\theta$r

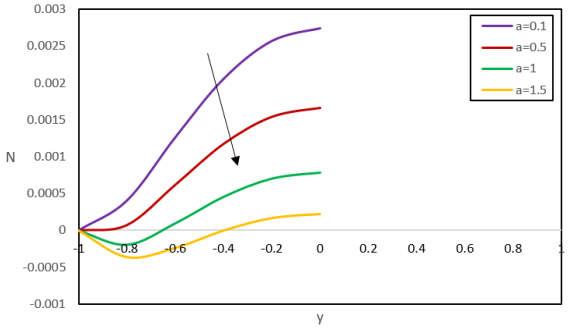


Fig. 17: Variation of angular velocity with thermal slip (a)

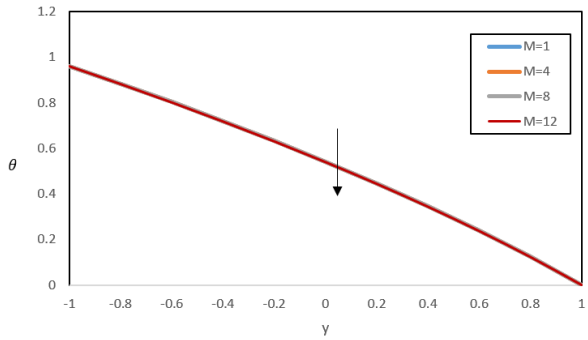


Fig. 18: Variation of temperature with M

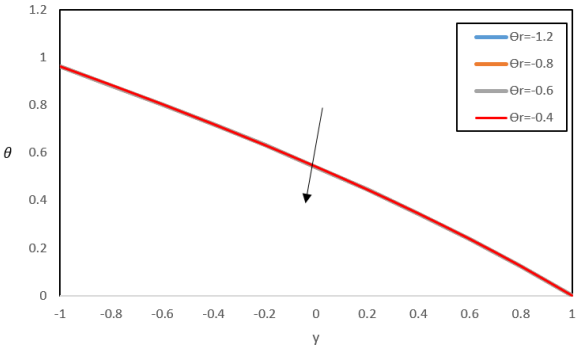


Fig. 19: Variation of temperature with $\theta$r

Figures 18–20 depict a scenario where a rise in the magnetic field parameter, Variable viscosity, and thermal slip corresponds to a decrease in temperature. The intricate interplay between magnetic forces, heat transfer, and thermal slip effects helps to explain this observed phenomenon. The heightened magnetic field parameter intensifies magnetic forces, impeding the fluid's efficient heat dissipation. Additionally, increased variable viscosity enhances the fluid's heat conduction capability, but the heightened thermal slip hinders the effective

transfer of this heat to the surrounding medium. Consequently, the cumulative impact of heightened magnetic field strength, improved variable viscosity, and increased thermal slip collectively results in a temperature decrease as the fluid faces challenges in dissipating heat effectively, leading to a cooling effect.

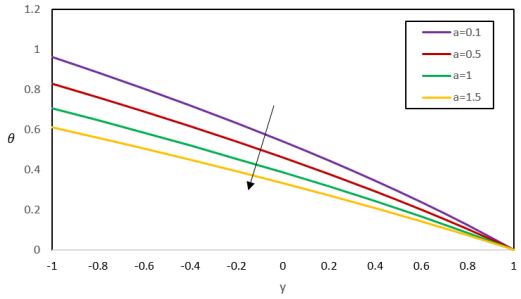


Fig. 20: Variation of temperature with thermal slip (a)

Figures 21-26 depict the impact of diffusion on the parameters. Figures 21–23 illustrate an escalation in the magnetic field parameter, thermal conductivity, and thermal slip is associated with an observed rise in diffusion. This phenomenon results from the intricate interplay of magnetic effects, heat transfer, and thermal slip. The heightened magnetic field parameter strengthens magnetic forces, influencing fluid molecular motion and aiding particle dispersion. Simultaneously, increased thermal conductivity improves heat conduction, facilitating widespread diffusion. Elevated thermal slip enhances fluid transport characteristics, enabling efficient particle dispersion. Higher magnetic field strength, better thermal conductivity, and higher thermal slip all work together to improve diffusion by making it easier for particles to move around and for heat to move through the fluid. In figures 24-26, an increase in Reynolds number (R), Sorret number (Sr), and Smidth number (Sc) corresponds to a simultaneous decrease in diffusion. This phenomenon arises due to the intricate relationship among these parameters in fluid dynamics. A higher Reynolds number shows a shift to high turbulent flow, diminishing orderly motion crucial for efficient diffusion. Elevated Sorret number (Sr) and Smidth number (Sc) enhance thermal effects, impeding molecular motion crucial for diffusion. The collective impact of increased Reynolds number, Sorret number, and Smidth number collectively impedes diffusion by disrupting fluid movement and hindering the thermal processes necessary for effective particle dispersion.

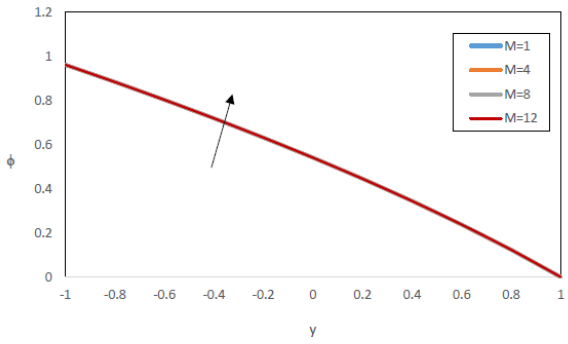


Fig. 21: Variation of diffusion with M

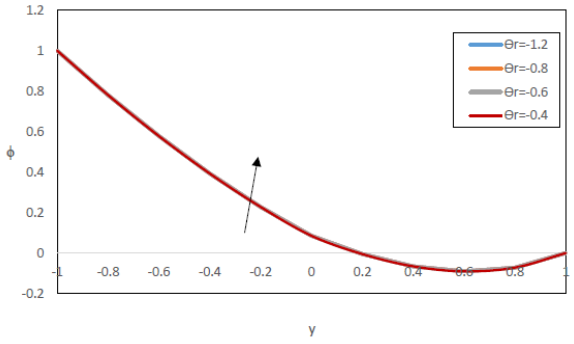


Fig. 22: Variation of diffusion with $\theta$r

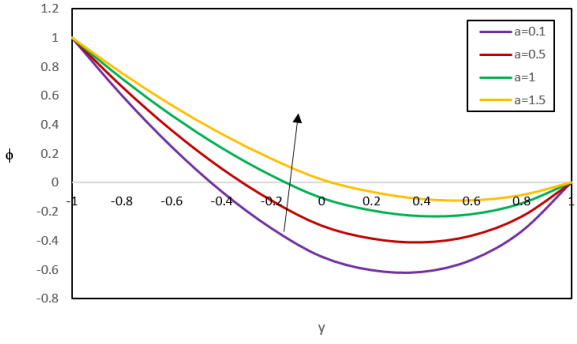


Fig. 23: Variation of diffusion with thermal slip (a)

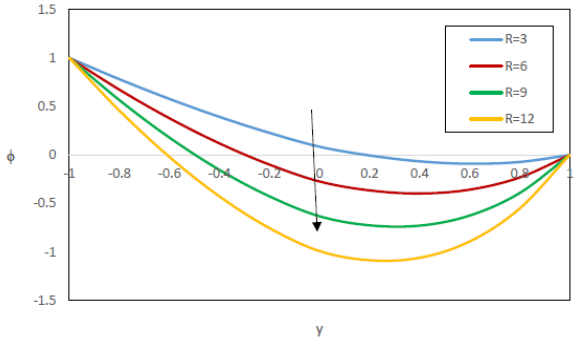


Fig. 24: Variation of diffusion with R

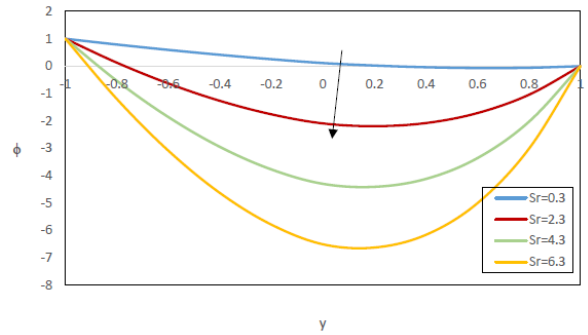


Fig. 25: Variation of diffusion with Sr

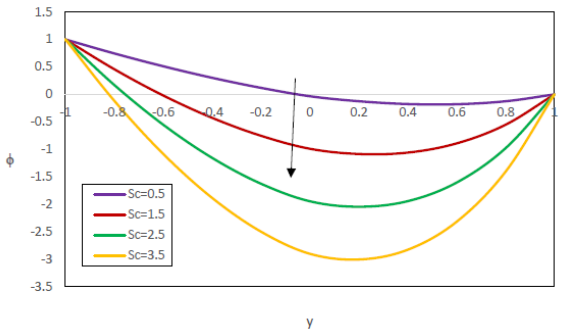


Fig. 26: Variation of diffusion with Sc

Figure 27 illustrates several relationships between different parameters and shear stress values (st1 and st2). An increase in Grashof number corresponds to an increase in shear stress, as higher Grashof numbers typically indicate stronger buoyancy forces, influencing fluid motion. Similarly, a rise in molecular Grashof number (Gc), representing buoyancy effects due to temperature differences, leads to higher shear stress values. The impact of the Reynolds number on the shear stress depends on flow regime, with higher Reynolds numbers generally resulting in increased shear stress. Sorret number (Sr) shows an inverse relationship with shear stress, indicating that higher Sr values may lead to a reduction in the effects of buoyancy or thermal gradients. An increase in Smidth number (Sc) results in a decrease in shear stress, suggesting a decrease in the importance of thermal diffusion effects. The magnetic field parameter (M) displays a suppressive effect on shear stress, as increasing M values correspond to decreasing shear stress values. Moreover, variable viscosity ($\theta$r) plays a role in shear stress, with less negative values of $\theta$r leading to an increase in shear stress. This suggests that materials with a greater ability to conduct heat exhibit higher shear stress. Conversely, a leads in thermal slip (a) corresponds to a reduction in shear stress, as higher values of thermal slip indicate reduced resistance to heat flow across the material, resulting in lower shear stress. Overall, these observations highlight the complex interplay between various parameters and shear stress in different physical systems.

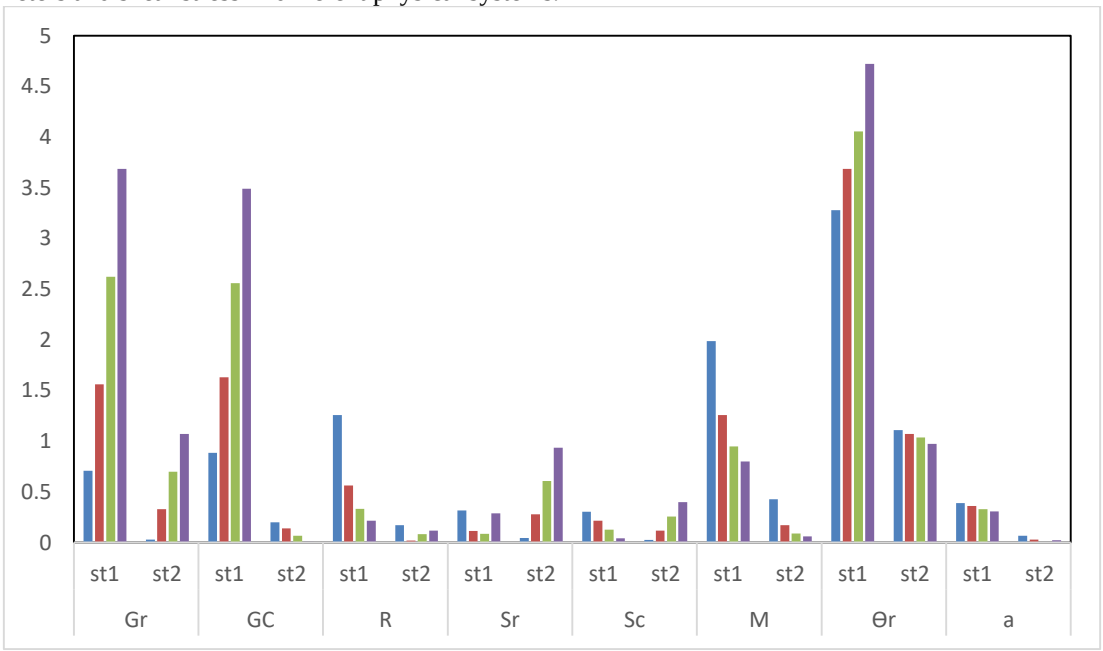


Fig. 27: Shear stress values for both the walls

Figure 28 depicts an increasing Grashof and molecular Grashof numbers from 1 to 15 which leads to a general reduction in Nusselt numbers (nu-1 and nu-2), indicating an inverse relationship. The impact of the Reynolds number on nu-1 shows a decreasing trend from 3 to 12, while nu-2 exhibits a more complex pattern. Higher Sorret and magnetic field parameters result in lower Nusselt numbers, implying reduced heat transfer efficiency. The connection between the Schmidt number and the Nusselt number is less clear. Moreover, as variable viscosity ($\theta$r) approaches zero, nu-1 and nu-2 increase, suggesting a positive correlation. Conversely, an increase in thermal

slip (a) from 0.1 to 1.5 leads to a significant decrease in Nusselt numbers, indicating an inverse relationship and reduced effectiveness of heat transmission.

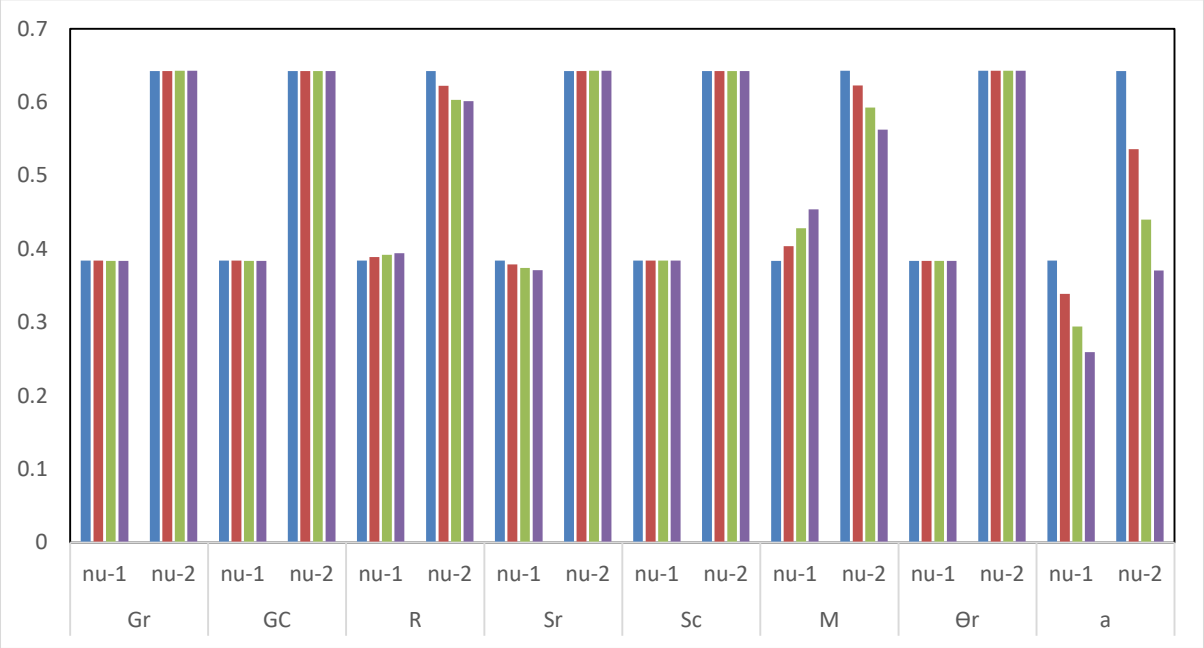


Fig. 28: Nusselt number values for both the walls

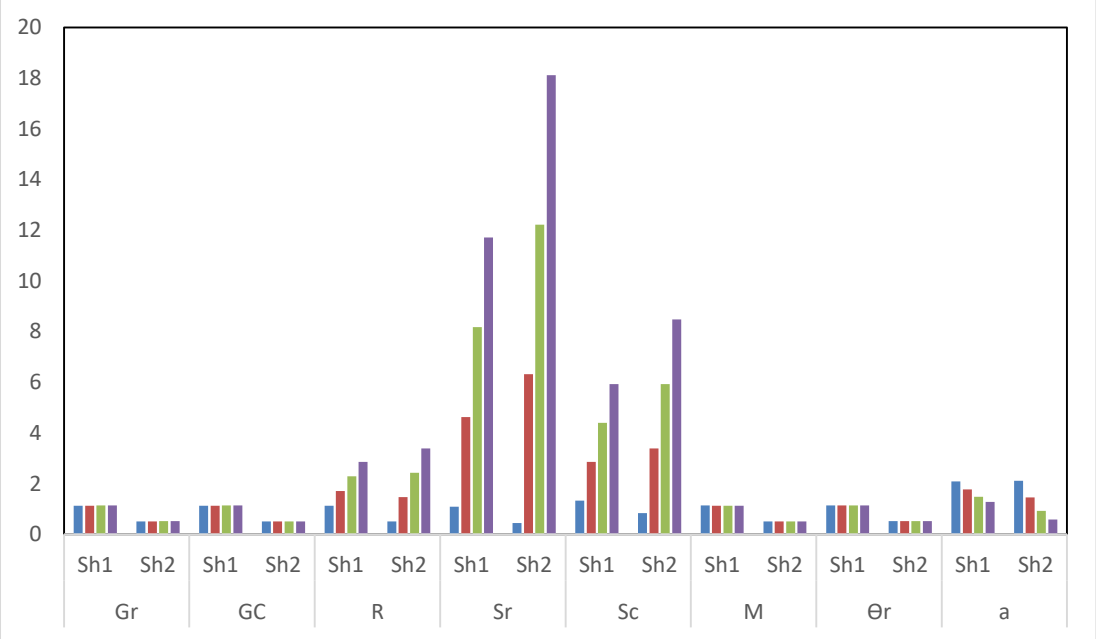


Fig. 29: Sherwood values for both the walls

Figure 29 illustrates consistent behavior in Shearwood numbers ($Sh_1$ and $Sh_2$) as Grashof number increases, showing minimal variation. The influence of molecular Grashof number (Gc) on Sherwood numbers is limited. However, Sherwood numbers exhibit significant changes with increasing Reynolds number, demonstrating a pronounced effect. As Sorret number (Sr) rises, a noteworthy increase in Sherwood numbers is noted, indicating a positive correlation. The relationship between Smidth number (Sc) and Sherwood numbers is evident, with an increase in Sc leading to a substantial rise in $Sh_1$ and $Sh_2$. The magnetic field parameter (M) exerts a negligible influence, resulting in a slight decrease in Shearwood numbers. Additionally, the inverse relationship between variable viscosity ($\theta$r) and Sherwood numbers suggests that materials with higher thermal conductivity have lower Sherwood numbers. Moreover, an increase in thermal slip (a) corresponds to lower Sherwood numbers, reflecting

reduced shear stress. Overall, these findings emphasize the intricate interplay of various parameters influencing Sherwood numbers in the examined physical systems.

## 5. Conclusions

The outcomes of the study upon the implementation of aforesaid physical parameters:

- The Grashof number (Gr), molecular Grashof number (Gc), and variable viscosity ($\theta$r) lead to increased fluid velocity. Due to buoyant and viscous forces.
- A reduction in fluid velocity with increased magnetic field parameter (M), Reynolds number (R), Sorret number (Sr), Smidth number (Sc), and thermal slip (a).
- When the molecular Grashof number (Gc), magnetic parameter (M), Reynolds number (R), Soret number (Sr), Schmidt number (Sc), and thermal conductivity all go up, the angular velocity also goes up.
- A decrease in angular velocity with increased Grashof number and thermal slip is due to hindered heat transfer and reduced buoyancy-driven forces.
- A rise in thermal conductivity, magnetic field parameter, and thermal slip results in a reduction in temperature.
- Increased thermal conductivity enhances heat conduction, but heightened thermal slip hinders effective transfer, resulting in a cooling effect.
- A rise in thermal conductivity, magnetic field parameter, and thermal slip leads to a rise in diffusion.
- Enhanced thermal slip improves fluid transport characteristics, enabling efficient particle dispersion and contributing to increased diffusion.
- A rise in Reynolds number (R), Sr, and Sc corresponds to reduction in diffusion.
- Variable viscosity ($\theta$r) influences shear stress, less negative $\theta$r values lead to increased shear stress.
- Increase in thermal slip (a) corresponds to reduced shear stress, indicating lower resistance to heat flow.
- As Variable viscosity ($\theta$r) approaches zero, Nusselt numbers increase, suggesting a positive correlation.
- A rise in thermal slip (a) leads to a significant reduction in Nusselt numbers, indicating an inverse relationship and reduced heat transmission effectiveness.
- Inverse relationship between variable viscosity ($\theta$r) and Sherwood numbers, suggesting higher thermal conductivity leads to lower Sherwood numbers.
- Increase in thermal slip (a) corresponds to lower Sherwood numbers, reflecting reduced shear stress.

## References

Abbas, N., Khan, W., Asjad, M. I., Sajid, M., and Siddique, I. (2023): Velocity and thermal slips impact on boundary layer flow of micropolar nanofluid over a vertical nonlinear stretched Riga sheet, Proceedings of the Institution of Mechanical Engineers, Part N, Journal of Nanomaterials, Nanoengineering and Nanosystems. https://doi.org/10.1177/23977914231156685

Alyousef, H. A., Saleem, S., Khan, I., Malik, M. Y., and Bhatti, M. M. (2023): Mathematical modeling and analysis of the steady electro-osmotic flow of two immiscible fluids, A biomedical application, Coatings, Vol. 13, No. 1, 115. https://doi.org/10.3390/coatings13010115

Babu, B. S., Srinivas, G., and Reddy, B. R. K. (2011): Finite element analysis of free convection flow with MHD micropolar and viscous fluids in a vertical channel with dissipative effects, Journal of Naval Architecture and Marine Engineering, Vol. 8, No. 1, pp. 59–69. https://doi.org/10.3329/jname.v8i1.5808

Bandari, S., and Perati, M. R. (2023): Study of radial vibrations in a fluid-filled poroelastic cylindrical bore saturated with two immiscible fluids, ZAMM–Journal of Applied Mathematics and Mechanics/Zeitschrift für Angewandte Mathematik und Mechanik, Vol. 103, No.5. https://doi.org/10.1002/zamm.202100547

Bashir, S., and Sajid, M. (2023): Flow of two immiscible uniformly rotating micropolar and viscous fluid layers, ZAMM–Journal of Applied Mathematics and Mechanics/Zeitschrift für Angewandte Mathematik und Mechanik, Vol. 103, No.11. https://doi.org/10.1002/zamm.202200371

Baitharu, A. P., Sahoo, S., and Dash, G. C. (2021): Effect of joule heating on steady MHD convective micropolar fluid over a stretching/shrinking sheet with slip flow model, Journal of Naval Architecture and Marine Engineering, Vol. 18, No. 2, pp. 175–186. https://doi.org/10.3329/jname.v18i2.55253

Cheruku, V., and Reddy, B. R. (2023): Numerical analysis of heat and mass transfer in a vertical channel with multiple slip effect, International Journal on Interactive Design and Manufacturing (IJIDeM), Vol. 18, No.5, pp.3155–3165. https://doi.org/10.1007/s12008-023-01471-w

Cheruku, V., and Reddy, B. R. (2023): Numerical study in effect of thermal slip on two-fluid flow in a vertical channel, Transactions on Energy Systems and Engineering Applications, Vol. 4, No. 2, pp. 1–18. https://doi.org/10.32397/tesea.vol4.n2.517

Farooq, M., Shah, F., Khan, M., Raza, M., and Alsaedi, A. (2024): A study of heat and mass transfer flow of a variable viscosity couple stress fluid between inclined plates, Modern Physics Letters B, Vol. 38, No. 9. https://doi.org/10.1142/S0217984923502317

Farooq, U., Rashid, A., Imran, M., Mushtaq, M., Rauf, A., and Khan, M. (2014): Heat and mass transfer of two-layer flows of third-grade nano-fluids in a vertical channel, Applied Mathematics and Computation, Vol. 242, pp. 528–540. https://doi.org/10.1016/j.amc.2014.05.126

Ganesh, N. V., Al-Mdallal, Q. M., and Chamkha, A. J. (2019): A numerical investigation of Newtonian fluid flow with buoyancy, thermal slip of order two, and entropy generation, Case Studies in Thermal Engineering, Vol. 13, 100376. https://doi.org/10.1016/j.csite.2018.100376

Goud, B. S., Sastry, V. S. B., Raju, C. S. K., and Chamkha, A. J. (2022): Thermal radiation impact on magneto-hydrodynamic heat transfer micropolar fluid flow over a vertical moving porous plate, A finite difference approach, Journal of the Indian Chemical Society, Vol. 99, No. 8, 100618. https://doi.org/10.1016/j.jics.2022.100618

Hazarika, G. C., and Konch, J. (2016): Effects of variable viscosity and thermal conductivity on magnetohydrodynamic free convection dusty fluid along a vertical porous plate with heat generation, Turkish Journal of Physics, Vol. 40, No. 1, pp. 52–68. https://doi.org/10.3906/fiz-1509-14

Hazarika, G. C., and Phukan, B. (2016): Effects of variable viscosity and thermal conductivity on magnetohydrodynamic free convection flow of a micropolar fluid past a stretching plate through porous medium with radiation, heat generation, and Joule dissipation, Turkish Journal of Physics, Vol. 40, No. 1, pp. 40–51. https://doi.org/10.3906/fiz-1508-21

Huang, H., Shaheen, S., Nisar, K. S., & Arain, M. B. (2024): Thermal and concentration analysis of two immiscible fluids flowing due to ciliary beating, Ain Shams Engineering Journal, Vol. 15, No. 1, 102278. https://doi.org/10.1016/j.asej.2023.102278

Hwang, J.H., Lee, S., Park, C., and Kim, H. (2024): Condensation heat transfer in the presence of non-condensable gases on a vertical tube bundle, International Communications in Heat and Mass Transfer, Vol. 152, 107239. https://doi.org/10.1016/j.icheatmasstransfer.2024.107239

Jabeen, K., Shah, Z., Khan, Z., and Yousaf, Z. (2024): A numerical study of boundary layer flow of Williamson nanofluid in the presence of viscous dissipation, bioconvection, and activation energy, Numerical Heat Transfer, Part A: Applications, Vol. 85, No. 3, pp. 378–399. https://doi.org/10.1080/10407782.2023.2187494

Kalyan, S., Sharan, A., and Chamkha, A. J. (2023): Heat and mass transfer of two immiscible flows of Jeffrey fluid in a vertical channel, Heat Transfer, Vol. 52, No. 1, pp. 267–288. https://doi.org/10.1002/htj.22694

Khan, I., Hussain, S., Zubair, M., and Shah, Z. (2024): MHD flow of third-grade fluid through a vertical micro-channel filled with porous media using semi-implicit finite difference method, Alexandria Engineering Journal, Vol. 86, pp. 513–524. https://doi.org/10.1016/j.aej.2023.11.070

Khan, K. A., Ali, N., Hussain, S., and Bilal, M. (2023): Heat and mass transport analysis for Williamson MHD nanofluid flow over a stretched sheet, Results in Physics, Vol. 53, 106873. https://doi.org/10.1016/j.rinp.2023.106873

Kho, Y. B., Pop, I., Aziz, N. A. M., and Salleh, Z. (2019): Heat and mass transfer analysis on flow of Williamson nanofluid with thermal and velocity slips: Buongiorno model, Propulsion and Power Research, Vol. 8, No. 3, pp. 243–252. https://doi.org/10.1016/j.jppr.2019.01.011

Kiran Kumar, G., Srinivas, G., and Babu, B. S. (2019): Effects of viscosity, thermal conductivity, and heat source on MHD convective heat transfer in a vertical channel with thermal slip condition, in Recent Trends in Wave

Mechanics and Vibrations, Select Proceedings of WMVC 2018, 71–86, Singapore: Springer Singapore. https://doi.org/10.1007/978-981-15-0287-3_6

Leclaire, S., Reggio, M., and Trépanier, J.-Y. (2013): Progress and investigation on lattice Boltzmann modeling of multiple immiscible fluids or components with variable density and viscosity ratios, Journal of Computational Physics, Vol. 246, pp. 318–342. https://doi.org/10.1016/j.jcp.2013.03.039

Mahmood, Z., Shehzad, S. A., Ilyas, A., and Raza, M. (2024): Analysis of mixed convective stagnation point flow of hybrid nanofluid over a sheet with variable thermal conductivity and slip conditions: A model-based study, International Journal of Heat and Fluid Flow, Vol. 106, 109296. https://doi.org/10.1016/j.ijheatfluidflow.2024.109296

Makinde, O. D. (2012): Effect of variable viscosity on thermal boundary layer over a permeable flat plate with radiation and a convective surface boundary condition, Journal of Mechanical Science and Technology, Vol. 26, No.5, pp. 1615–1622. https://doi.org/10.1007/s12206-012-0302-1

Malapati, V., and Lakshmi, D. V. (2021): Diffusion-thermo and heat source effects on the unsteady radiative MHD boundary layer slip flow past an infinite vertical porous plate, Journal of Naval Architecture and Marine Engineering, Vol. 18, No. 1, pp. 55–72. https://doi.org/10.3329/jname.v18i1.33024

Pal, D., and Mondal, H. (2014): Influence of variable viscosity on hydromagnetic non-Darcy convective-radiative heat transfer over a stretching sheet with non-uniform heat source/sink, International Journal for Computational Methods in Engineering Science and Mechanics, Vol. 15, No. 6, pp. 490–498. https://doi.org/10.1080/15502287.2014.934489

Potyka, J., and Schulte, K. (2024): A volume of fluid method for three-dimensional direct numerical simulations of immiscible droplet collisions, International Journal of Multiphase Flow, Vol. 170, 104654. https://doi.org/10.1016/j.ijmultiphaseflow.2023.104654

Reddy, N. N., Bandari, S., and Al-Mdallal, Q. M. (2023): Impact of porosity and radiation on two-dimensional unsteady magnetohydrodynamics heat transfer stagnation point flow with viscous dissipation, Heat Transfer, Vol. 52, No. 5, pp. 3538–3556. https://doi.org/10.1002/htj.22839

Shah, F., Khan, M., Farooq, M., Raza, M., and Alsaedi, A. (2024): Heat transfer analysis on MHD flow over a stretchable Riga wall considering entropy generation rate, A numerical study, Numerical Methods for Partial Differential Equations, Vol. 40, No. 1. https://doi.org/10.1002/num.22694

Suresh Babu, B., Srinivas, G., and Srikanth, G. V. P. N. (2019): Finite element study of convective heat and mass transfer of two fluids in a vertical channel of variable width with Soret and Dufour effects, in Numerical Heat Transfer and Fluid Flow, Select Proceedings of NHTFF 2018, 537–546. Singapore: Springer Singapore. https://doi.org/10.1007/978-981-13-1903-7_62

Ullah, Z., and Alkinidri, M. (2023): Effect of variable viscosity on oscillatory heat and mass transfer in mixed convective flow with chemical reaction along inclined heated plate under reduced gravity, Alexandria Engineering Journal, Vol. 77, pp. 539–552. https://doi.org/10.1016/j.aej.2023.07.023

Xu, H., Wang, T., and Che, Z. (2024): Coalescence of immiscible droplets in liquid environments, Journal of Colloid and Interface Science, Vol. 659, pp. 60–70. https://doi.org/10.1016/j.jcis.2023.12.103